Satellite-Derived Approaches for Coal Mine Methane Estimation: A Review

Akshansha Chauhan[1], Simit Raval[1, *]

1 School of Minerals and Energy Resources Engineering, University of New South Wales, Sydney, NSW, Australia,

Emails: akshansha.chauhan@unsw.edu.au; simit@unsw.edu.au;

*Correspondence: simit@unsw.edu.au;

Review

Satellite-Derived Approaches for Coal Mine Methane Estimation: A Review

Akshansha Chauhan[1], Simit Raval[1, *]

1 School of Minerals and Energy Resources Engineering, University of New South Wales, Sydney, NSW, Australia,

***** Correspondence: simit@unsw.edu.au;

Abstract:

Methane emissions from coal mines, especially surface operations, are spatially diffuse, presenting significant challenges for accurate quantification. Satellites such as TROPOMI, GHGSat, PRISMA, Gaofen-5, and GO-SAT have been extensively used for detecting methane emissions at various scales, from individual point sources to regional and global assessments. Despite various advancements, methane quantification via satellite observations remains subject to several challenges. Various quantification methods for the same observation can produce variable results. Also, meteorological conditions, terrain complexity, and surface heterogeneity introduce uncertainties in emission estimates. The selection of wind speed and direction, along with retrieval algorithm limitations, can lead to significant discrepancies in reported emissions. Additionally, satellite-based observations capture emissions only at specific overpass times, which may introduce temporal uncertainties compared to inventories derived from continuous emission estimations. This study provides a comprehensive review of satellite-based coal mine methane monitoring, evaluating current methodologies, their limitations, and recent technological advancements. We discussed the potential of emerging machine learning techniques, improved atmospheric modelling, and integrated observational approaches to enhance methane emission quantification. By refining satellite-based monitoring techniques and addressing existing challenges, this research will support the development of more accurate emission inventories and effective mitigation strategies for the coal mining sector.

Keywords: GHG Emissions, Coal mine methane, Satellite remote sensing, Methane inventories.

---

1. Introduction

Globally, the anthropogenic Greenhouse Gas (GHG) emissions are increasing due to the human induced activities [1-3]. IPCC has raised concerns for global GHG emissions as the past decade experienced a temperature rise of 1.1°C [4]. An increase in warming beyond 2 ºC could be devastating for the entire ecosystem [5], so the goal is to keep it well below the 2 ºC threshold, ideally around 1.5 ºC [6]. To this end, the Paris Agreement set a target of 43% reduction in GHG emissions by 2030 to achieve net-zero by 2050 [6]. However, current mitigation measures are not sufficient to keep the global temperature well within the target limit [7, 8] which further emphasises the increasing need of GHG emission mitigation efforts including improving detection and monitoring technologies.

Carbon dioxide (CO_2) and Methane (CH_4) are two major GHGs contributors to global warming and climate change [9]. Methane, though accounting for 18% of greenhouse gas emissions, has a warming potential 86 times greater than CO_2 over a 20-year period however it has a relatively short atmospheric lifetime of 12 years [4]. It is responsible for 30% of the current rise in global temperature [10]. So, mitigation of methane emission will help limit the atmospheric warming as well as improve air quality, because methane also

contributes to surface ozone formation, a key factor in air quality deterioration [11]. Various natural and anthropogenic sources impact the global methane budget; however, Energy and Agriculture related emissions are together cause more than 60% of total methane budget [12, 13]. Fugitive emissions from the energy sector alone contribute approximately 32% (ranging from 22% to 42%) of total global methane emissions, stemming from oil and gas operations, coal mining, and other sources [4]. These emissions originate from a variety of sources, ranging from small point sources such as leaks and flaring, to broader area sources such as surface coal mines and landfills exhibiting highly variable flux rates, from a few kilograms per hour (kg/h) to several tonnes per hour (t/h). Emissions from oil and gas leaks have attracted considerable attention due to their direct commercial implications for operators, leading to the rapid development of advanced quantification technologies. In contrast, methane emissions from coal mines face unique challenges in both capture and observation and have consequently received relatively limited focus. Existing observation techniques often struggle to quantify fugitive emissions accurately due to limitations in spatial and temporal coverage, model uncertainties, and operational feasibility constraints. Therefore, it is essential to develop and implement robust strategies for Monitoring, Measurement, and Mitigation tailored to these diverse and often underrepresented emission sources.

Coal is a major source of energy as still it is the highest contributor among all other conventional energy sources and hence caused 33% of global CO_2 emission by 2019 [4]. The coal mining fugitive emissions of methane appears to be between 0.1 and 0.2 $GtCO_2$-eq/yr for the period 2010–2019 [4]. As per IEA 2024 report, coal caused 6.85 % to total global CH_4 emissions [13]. During the coalification process, methane is generated primarily due to biological activity at early stages (biogenic methane) and thermal decomposition of organic matter at later stages (thermogenic methane) and becomes trapped in the coal seams [14]. Methane is predrained from boreholes drilled into the seam prior to mining to reduce in-situ gas pressure and enhance operational safety. The amount of extractable methane depends on factors such as coal type, depth of the seam, and geological conditions [15]. Mining activities further facilitate the release of methane through diffuse emissions generally referred to as Coal Mine Methane (CMM). The gas content increases with the depth of the coal seam, leading to generally higher methane emissions from deep-seated coal deposits [15]. To mitigate explosion risks during mining operations in an underground mine, since methane-air mixtures become explosive at concentrations of 5%, ventilation systems are used to maintain methane concentrations below 2% in the confined underground environment [16]. So, the ventilation air methane (VAM) behaves as a point source and has higher possibility to be detected as well as quantified using existing techniques. However, methane emissions from surface mines present significant challenges due to the diffuse and multifaceted nature of their sources. In surface mining, activities such as drilling, blasting, excavation, transportation, washing and stockpiling as well as emissions from the exposed coal in the pits itself contribute to CMM. The diverse and dispersed nature of these sources makes quantification and mitigation particularly complex [16].

In recent years, a range of observation technologies has rapidly evolved to monitor methane emissions. Key technologies include infrared imaging, laser absorption spectroscopy methods such as TDLAS and DIAL, metal oxide sensors, cavity ring-down spectroscopy (CRDS), non-dispersive infrared (NDIR) sensors, ground- and aerial-based passive SWIR spectroscopy, and Fourier-transform infrared spectroscopy (FTIRS) [17]. Ground observations methods often have higher accuracy with better temporal coverage but limited spatial coverage. Remote sensing instruments, on the other hand, have higher spatial coverage with point to area emissions observations [18]. Observation of methane is conducted using satellite, aerial, UAV and ground-based sensors, each with its own detection limits and constraints. Satellite remote sensing of methane particularly is a cost-effective approach with higher spatial coverage [18]. Most satellites estimate atmospheric methane using passive remote sensing in the shortwave infrared (SWIR) spectrum, where methane exhibits strong absorption features. However, the mid-wave infrared (MWIR) spectrum also shows sensitivity to atmospheric methane and can be used under certain conditions. However, it comes with various limitations such as cloud and aerosols constraints, lower resolution in comparison to the arial and UAV sensors and possibility of only daytime acquisitions. Figure 1 displays various current and future satellite mission for the dedicated methane observation and few tailored solutions due to their observations in SWIR band. GOSAT,

SCHAMECY, TROPOMI, MethaneSAT, Carbon Mapper and GHGSat are the current dedicated methane observation satellites, however, EMIT, EnMAP, PRISMA, Sentinel-2, LandSat, WorldView-3 and Gaofen-5 are the hyperspectral missions which can be utilized for methane plume detection. These satellites can also further categories as point source imagers and Area Flux mapper based on the swath of the satellite. The flux detection limits of the point source satellites are better than the area mapper, for example GHGSat can detect a flux rate close to 100 kg/h [19]. However, the area mapper such as TROPOMI is able to scan large scan and compromise the minimum detection limits but provide daily global coverage.

This manuscript focuses on satellite-based remote sensing of coal mine methane (CMM) emissions from 2015 to 2024. CMM emissions are typically diffuse, low in intensity, yet persistent over time. VAM emissions from underground mines sometimes fall under the 'super-emitter' category, with flux rates reaching several tons per hour [20]. In contrast, individual plumes from surface mines pose a challenge for satellite detection due to their relatively lower emission rates, often in the range of a few kilograms per hour [20]. Nevertheless, studies have reported that satellite-based measurements can effectively capture methane emissions at the basin scale. Therefore, it is essential to conduct comprehensive review of all the studies that reported the coal mine methane using satellite observations. In this review, we analyse research published over the past decade on coal mine methane observation, as indexed in the Scopus database. The emphasis of current study is to discuss the satellite capabilities, emission quantification techniques, and limitations of satellite observation. This analysis aims to provide the research community with a clearer understanding of the opportunities and limitations of satellite-based methane monitoring, enabling more informed interpretation and application of these observations.

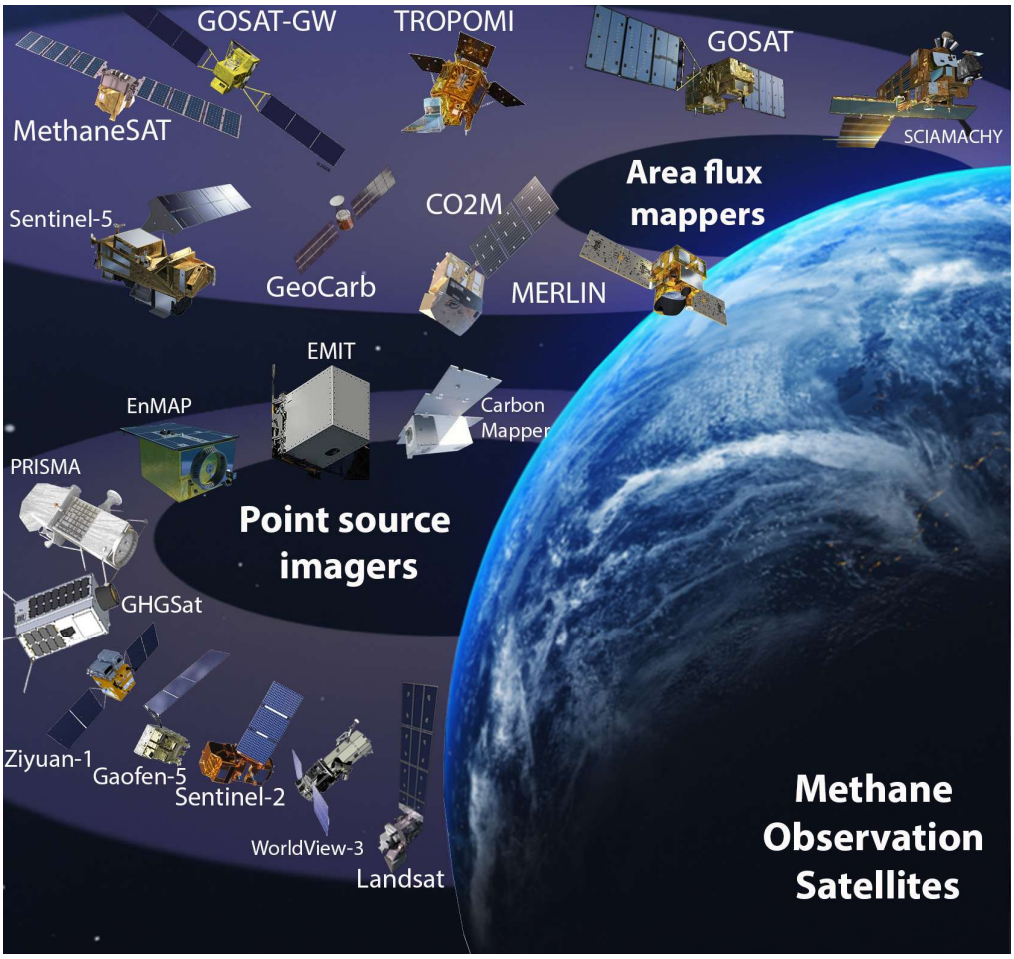

Figure 1: The methane observation satellite missions.

2. Materials and Methods

Based on the scope of the current review, we did the literature survey based on the Scopus databased using the key word "coal+mine+methane". Other search criteria are given in Table 1. During the past 10 years, satellite remote sensing technologies have been developed at rapid scale. Technology has enhanced from SCIAMACHY and GOSAT like sensors with revisit rate of several days to GHGSat constellations like point observers with pinpointing of leaks from gas pipelines. This review compiles satellite-based studies on coal mine methane emissions conducted between 2015 and 2024, highlighting observational efforts over the past decade. As per the SCOPUS databased, a total of 2117 articles were published in the past 10 years with the three key words (CMM). Large number of research papers focused on the detection of methane from mine safety perspective not for the emission quantification. Only 132 studies have been conducted to quantify CMM using various ground, arial and satellite-based observation techniques. In the present manuscript, we focus exclusively on satellite-based observations (Table 2), as they provide consistent, large-scale spatial and temporal coverage that is not feasible with ground or aerial methods. This focused approach allows for a more coherent comparison of methodologies and results within a single observational framework, avoiding inconsistencies that may arise from integrating fundamentally different measurement platforms.

For coal mine methane emission observations using satellite, there are only 21 research articles (Table 3) that were published. In our current review on methane emissions from coal mines, we have structured our analysis into key categories: types of sensors and satellites, data extraction and synthesis methods, evaluation of sensor capabilities, accuracy assessment, geographic distribution of studies, and validation of the results. This framework allows for a comprehensive examination of the available literature on coal mine methane quantification using satellite observations. This review aims to provide valuable insights for both the scientific community and policymakers to enhance their understanding towards the satellite based CMM quantification approaches.

Table 1: The search criteria for the current manuscript.

Item	Source
Database	Scopus
Seach Title	coal AND mine AND emission
Focus group	Satellite Observations
Time range	2015 to 2024
Document Type	Article, Conference Paper, Review, Book Chapter, Letter, Editorial, Data paper
Language	English

3. Satellite Platforms used for CMM Observations

This section discusses remote sensing satellites used for space-based observations of coal mine methane emissions, along with various models and methods for quantifying emission rates. It also explores the techniques employed, their limitations, and the overall effectiveness of current observational approaches.

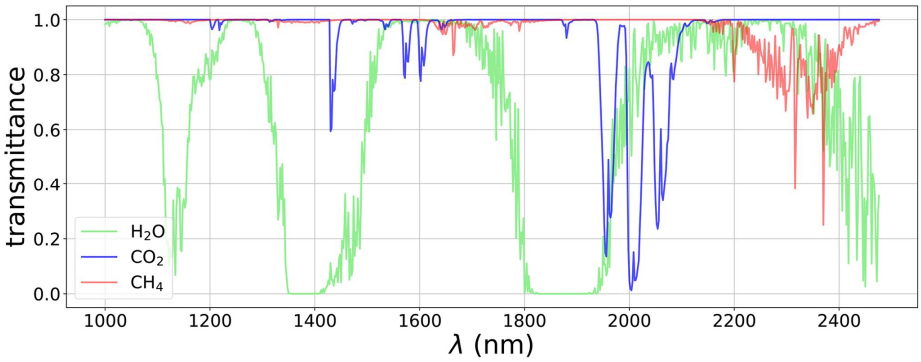

Figure 2: Transmittance spectra for atmospheric H_2O (green), CO_2 (blue), and CH_4 (red), generated using MODTRAN and resampled to a spectral resolution of 2 nm by Roger et al. [21].

Methane exhibits two absorption bands in the shortwave infrared (SWIR) region: a weaker band near 1700 nm and a stronger band around 2300 nm (Figure 2; [21]). Space borne shortwave infrared (SWIR) sensors with higher spectral resolution help in characterisation of earth surface, biosphere and atmospheric and estimation of chemical and physical properties [22 – 24]. Within the realm of spaceborne remote sensing, this improved spectral resolution has been leveraged across a variety of Earth observation fields from LULC changes to air quality. Atmospheric methane retrievals are performed in spectrally resolved observations of solar irradiation reflected off the Earth's atmosphere within SWIR spectrum, approximately 1.6 to 2.5 µm, and the MWIR spectrum, around 3.5 and 5 µm [25].

These absorption features are instrumental in satellite-based retrievals, enabling the estimation of column methane concentrations through atmospheric radiative transfer models (RTMs). SCIAMACHY and GOSAT were the two first atmospheric methane observation missions and with continuous development in sensor technologies, various missions are launched (Figure 1). Although satellites like Sentinel-2, WorldView-3, Gaofen-5, Landsat, EMIT, PRISMA, and EnMAP were not specifically designed for methane observations, their SWIR measurements have been successfully utilized for detecting and quantifying methane emissions [20, 26 - 28]. For coal mine methane (CMM) quantification, the most utilised satellite observations include those from TROPOMI, Gaofen-5, PRISMA, GHGSat-D, GOSAT, and IASI. In addition to these, observations from EMIT, EnMAP, and ZY1-02D have also been applied for CMM emission observation. The specifications and capabilities of these satellite platforms relevant to CMM monitoring are summarised in Table 2 and discussed in the following sections.

Table 2: List of satellites used for the coal mine methane emission observations and their specifications.

S. No.	Sensor Name	Revisit Rate	Type of Sensor	Methane Band	Resolution	Min Flux Rate	Swath Width
1	TROPOMI	1 Dfay	Hyperspectral Imaging	2.2 -2.4 µm	5.5 × 7 km	~10 t/h	2600 km
2	Gaofen-5	4-5 Days	Hyperspectral Imaging	2.11 - 2.45 μm	30 × 30 m	~1 t/h	60 km
3	PRISMA	2-3 Days	Hyperspectral Imaging	2.10 – 2.45 μm	30 × 30 m	~ 0.5 t/h	30 km
4	GHGSat-D	1 Day	Remote Sensing (Optical)	1.63−1.675 μm	25 × 25 m	~0.1 t/h	12 km
5	GOSAT	3 Days	Atmospheric Monitoring	1.65 µm	10 × 10 km²	~50 t/h	100 km

6	IASI (METOP)	12 Hours	Infrared Atmospheric Sounding	3.7-15 µm	5.5 × 7 km²	~0.1 Tg CH_4/year	2200 km
7	EnMAP	27 Days	Hyperspectral Imaging	2.10–2.45 µm	30 × 30 m	~1 t/h	30 km
8	Ziyuan-1	3 Days	Hyperspectral Imaging	2.10–2.45 µm	30 × 30 m	~1 t/h	115km
9	EMIT	Variable	Hyperspectral Imaging	2.10–2.45 µm	60 × 60 m	~1 t/h	75 km

3.1. TROPOMI

The TROPOspheric Monitoring Instrument (TROPOMI) instrument was co-funded by ESA and the Netherlands Key organizations from the Netherlands include KNMI (Royal Netherlands Meteorological Institute), SRON (Space Research Organization Netherlands), TNO (Netherlands Organization for Applied Scientific Research), and Airbus DS-NL, on behalf of NSO (Netherlands Space Office). KNMI and SRON are responsible for the development of Level 1B and some Level 2 products of satellite observation (e.g. Methane, Nitrogen Dioxide). With a swath width of 2600 km and spatial resolution of 5.5 x 7 km^2, it provides daily global coverage [29 – 31]. It carries out the observation of methane in the SWIR band at 2.3 µm (2314–2382 nm) (SRON CH4 L2 team, 2022). The local overpass time is around 1:30 PM for TROPOMI. Global methane observations from TROPOMI have been widely used to study coal mine methane (CMM) emissions in regions such as Poland, Australia, China, South Africa, and other parts of the world [28, 31- 40].

3.2. Gaofen-5

Gaofen-5 (GF 5) is part of China's civilian Earth observation satellite series under the China High-Definition Earth Observation System (CHEOS) program. It is designed for advanced remote sensing applications to support environmental monitoring, resource management, and other state-sponsored initiatives. GF 5 or GF 5A or GF 5-01 was the first satellite of Gaofen-5 series and GF 5-02 or GF-5B was the second satellite. The first satellite was launched on 08 May 2018, and the second satellite was launched on 7 September 2021. Gaofen-5 mission has several observation sensors form Hyperspectral imagers, Visible sensors, Atmospheric Infrared Ultra spectrometer, Directional Polarisation Camera, Environmental and GHG observation instruments. The Advanced Hyperspectral Imager (AHSI) on Gaofen-5 can capture images in a wide band ranging from 400 nm to 2500 nm, with a spatial swath of 60 km and a spatial resolution of 30 m [41, 42]. He et al. [43], Han et al. [44], and Bai et al. [26] utilized its 2100 to 2450 nm spectral window for column mass methane observations, focusing on CH_4 absorption features near 2300 nm. The local overpass time for Gaofan-5 is around 1:30 PM.

3.3. PRISMA

PRISMA (PRecursore IperSpettrale della Missione Applicativa) is a dedicated hyperspectral mission launched by Italian space agency for earth observations. The satellite can obtain the hyperspectral images with in ~400–2500 nm band with spatial resolution of 30 m and swath size of 30×30 km^2 [45]. The spectral resolution for PRIMA is not uniform, and it varies from 9 nm to 15 nm. The band near 2300 nm with spectral resolution of 10 nm can be used for the methane column mass inversions [46]. The inversion of the hyperspectral image for methane observations can be carried out in wavelength band from 2280nm to 2380nm as it is affected most by methane and water vapor absorption for PRISMA. The PRISMA satellite, operating in a sun-synchronous orbit, has a local overpass time of approximately 10:30 AM. PRISMA observations have been utilised for coal mine methane (CMM) estimation in Poland [21], China [21, 46], and rest of the world [28].

3.4. GHGSat- C/D

GHGSat-C/D are part of a constellation of small satellites designed for global methane observations. They were designed and operated by GHGSat Inc. for high-resolution methane observation, capable of detecting emissions as low as ~100 kg/h with high precision [47, 48]. With higher spatial resolution of 25 m × 25 m, and a 12 × 12 km^2 swath, GHGSat provide high resolution methane inversion results [18]. Using solar backscatter observations in the spectral range 1630–1675 nm of SWIR band, GHGSat-C/D are able to measure the atmospheric column methane. GHGSat-D has a mean return time of 2 weeks with an overpass time of 10:00 AM local solar time on ground. However, GHGSat-C has overpass time of 09:30 AM. The detailed technical discussion about the GHGSat satellites is discussed by Varon et al. [18]. GHGSat observations have been used for coal mine methane (CMM) estimation in the USA [20], Australia [20], and China [20, 26], as well as for global plume detection [28].

3.5. GOSAT

GOSAT is a JAXA mission within Japan's GCOM (Global Change Observation Mission) programme designed to monitor the global distribution of carbon dioxide and methane. GOSAT (Greenhouse gases Observing SATellite) is an environment-monitoring satellite developed by Japan which launched on 23 January 2009 and remains operational. It is part of ESA's Third-Party Missions Programme, in which ESA has an agreement with JAXA to distribute data products from the mission. Thermal and Near Infrared Sensor for Carbon Observation (TANSO) - onboard GOSAT consists of two instruments: the TANSO-FTS that observes the greenhouse gases; and the other is the TANSO-CAI that senses clouds and aerosols. The satellite has a sun-synchronous polar orbit with local pass time of 01:00 PM. GOSAT-1 performs nadir measurements of solar backscatter in the SWIR spectrum to retrieve methane column densities (1.65 μm), with high sensitivity in the troposphere and weaker sensitivity in the stratosphere [49]. The satellite observes three circular pixels, each 10 km in diameter, spaced 260 km apart along the orbit track. It samples the same locations every three days with global coverage. GOSAT observation helped in the development of methane emission observation and trend estimation. Miller et al. [50], Sheng et al. [51] and Zhang et al. [52] investigated the methane emission trends in China using GOSAT observations.

3.6. IASI (METOP)

The Infrared Atmospheric Sounding Interferometer (IASI) is a nadir-viewing Fourier-transform spectrometer (FTS) installed on METOP satellites (A, B, and C). Operating within the MWIR band (3.7-15 μm), IASI exhibits high sensitivity, particularly in the middle troposphere and stratosphere. It offers a spatial resolution of approximately 12 km and covers a swath width of 2200 km, with an equatorial overpass occurring at 09:30 and 21:30 local time. With nearly 14 orbits per day, IASI data has been extensively utilised for trace gas profiling [53 – 56]. Tu et al. [39] presented the observation of the tropospheric methane using IASI observation coupled with TROPOMI.

3.7. Other Point observations satellites

EMIT (Earth Surface Mineral Dust Source Investigation), EnMAP (Environmental Mapping and Analysis Program), and Ziyuan-1 02D are hyperspectral imaging missions not originally designed for methane detection but have recently been utilised for methane observations due to their high spectral resolution in the shortwave infrared (SWIR) range. EMIT, operated by NASA aboard the International Space Station, captures data in the 980–2130 nm range with a spatial resolution of ~60 m and has been used to detect strong methane plumes. EnMAP, operated by DLR, covers 420–2450 nm with 30 m spatial resolution and a swath of 30 km, offering daytime overpasses at around 11:00 AM local time, it has demonstrated utility in capturing methane enhancements over coal mines under suitable conditions. ZY1-02D, launched by China with the Advanced Hyperspectral Imager (AHSI), provides 30 m resolution over a 60 km swath in the 400–2500 nm range and used in methane analysis, particularly in a study over Shanxi, China [26]. While these missions are not dedicated to methane monitoring, their SWIR observations are being exploited for high-resolution CMM detection and analysis.

4. Methods used for CMM quantifications

The quantification of methane emissions, particularly flux estimation, involves multiple steps (Figure 3). Satellites observe spectrally resolved solar radiation reflected from the Earth's surface and atmosphere in the shortwave infrared (SWIR) spectrum, which is processed as Level 1 radiance data. Using radiative transfer models (RTMs), this spectral information is inverted to retrieve the column-averaged dry-air mole fraction of methane (XCH_4), typically referred to as Level 2 data. Subsequently, XCH_4 data are used to estimate emission rates or fluxes through various approaches, such as mass balance, plume inversion, or data assimilation techniques. This section covers the methodologies used in the studies so far for estimating CMM fluxes using satellite-based observations.

4.1. Inversion Methods

The inversion of raw satellite radiances (Level 1) to column-averaged dry-air mole fraction of methane (XCH_4) or Level 2 data involves various inversion techniques. A clear-sky radiative transfer model is integrated within an inverse modelling framework to retrieve methane concentrations from satellite-based imaging spectroscopy data. These methods primarily rely on radiative transfer processes occurring between the atmosphere, and the observing instrument. RemoTeC full-physics algorithm was first developed for GOSAT [57 – 59] and later was also utilised for TROPOMI observations for column mass concentration of methane [39]. For CMM observations, RemoTeC retrieved dry-air column mass methane (XCH_4) observation has been applied in 13 studies for TROPOMI and GOSAT inversions [28, 32 – 40, 50 – 52]. For TROPOMI, the model atmosphere is divided into 36 uniform vertical layers, with input profiles of trace gases and meteorological parameters sourced from ECMWF data. The retrieval algorithm relies on spectral bands specifically the Near Infrared (NIR) and Short-Wave Infrared (SWIR) to extract aerosol information. In the NIR band, O_2 absorption features are used, while in the SWIR band, absorption by CH_4 and H_2O provides sensitivity to aerosol scattering effects. These spectral regions allow for the retrieval of aerosol amount, size, and height, which are simultaneously estimated along with methane columns to account for aerosol-induced light path modifications. GHGSat applies an inversion algorithm built on a simplified radiative transfer equation, incorporating high-resolution absorption line data from the HITRAN database and using vertical profiles based on the U.S. Standard Atmosphere, discretised into 100 equally spaced atmospheric layers for radiative transfer modelling [48]. GHGSat inversion models exclude thermal emission and molecular scattering effects in their atmospheric radiative transfer modelling, as these contributions are minimal within the instrument's SWIR spectral bandpass. This simplified GHGSat inversion model is referred to as radiative transfer modelling (RTM). Data driven Match Filter technique [46, 60, 61] was utilised to convert the spectra directly into plume enhance figure and this technique is utilised for GaoFan-5B and PRISMA observations by Bai et al. [26], Han et al. [44], He et al. [43] and Roger et al. [62]. The matched-filter retrieval approach is a data-driven technique that offers various key benefits over traditional full-physics and simplified radiative models. One of its primary strengths is its robustness against radiometric and spectral distortions, such as vertical striping caused by detector inconsistencies which often affect satellite observations. By operating on a pixel- or column-level basis, matched-filter methods effectively manage these systematic errors without the need for complex correction schemes [46]. Moreover, they facilitate the direct retrieval of methane concentration anomalies (ΔXCH_4), whereas full-physics approaches typically require additional steps, including background estimation, to derive similar outputs. Matched-filter retrievals are also significantly more computationally efficient, making them well-suited for large-scale processing. In contrast, full-physics models, while offering detailed atmospheric characterisation, are computationally demanding and more susceptible to uncertainties in model inputs. However, matched-filter approaches face limitations due to their reliance on basic linear signal frameworks, which fail to encapsulate the intricate physical mechanisms involved in detecting gases. Consequently, they can lead to substantial retrieval inaccuracies and exhibit a tendency to produce numerous false positives [46].

4.2. Wind observations

Wind is one of the key parameters for the column mass concentration data to estimation of the source rate conversion along with the plume shape. Equation 1, displays a simple mass balance approach for the estimation of the source rate or flux rate of methane for a satellite observation:

$$Flux\ rate_{CH_4} = \int_{-y}^{+y} \int_{-x}^{+x} \Delta XCH_4 \times U_{\text{eff}}\, dx\, dy \quad (1)$$

Here, ΔXCH_4 is the enhancement in dry-air column methane (or the anomaly) calculated by subtracting the background or upwind dry-air column methane concentration from the concentration in the downwind pixel, U_{eff} is the perpendicular effective wind speed, and x and y are the dimensions of the plumes. For oil and gas sources, plume lifetime is typically around 5 minutes, whereas for coal mines, plumes can persist for up to 1 hour [20]. Therefore, effective wind speed is calculated by averaging wind data over a specific time depending on the type of source, plume size and duration [20]. Most studies employing the mass balance approach for flux rate estimation determine effective wind based on the methodology outlined by Varon et al. [20]. It is also worth noting that the altitude of the wind is a key parameter. Varon et al. [20] calculated the effective wind by averaging the wind at 10 m. Wind information is also helpful to validate the plume by comparing the plume alignment with the available wind direction. For global wind data, satellite observations depend on the global meteorological reanalysis products. NASA Goddard Earth Observing System-Fast Processing (GEOS-FP) reanalysis and European Centre for Medium-Range Weather Forecasts (ECMWF) Reanalysis v5 (ERA5), which is the fifth generation ECMWF reanalysis product [63], are the two main reanalysis products which were used for emission estimations.

To obtain effective wind in mass balance equation, 10 m wind was most used by GOES-FP in 6 studies [20, 26, 28, 44, 46, 62]. However, ERA5 wind at 10 m, 100 m, 300 m, 1000 m and 1500 m was used for flux rate estimates by Schuit et al. [28], Hu et al. [32], Tu et al. [36, 39], Sadavarte et al. [40] and He at al. [43. The high-resolution satellite observations, Varon et al. [20], Bai et al. [26], Schuit et al. [28], Han et al. [44], He et al. [44], Roger et al. [62], Guanter et al. [46] and Ayasse et al. [64] used 10 m winds for effective wind analysis and flux estimates.

Palmer et al. [34] used 10m wind while applying simple mass balance approach for emission quantification for Australian coal mine region and did not consider the variable elevation of coal mine region and wide swath of TROPOMI. However, others consider these limitations while carrying out the effective wind and used 100m to 1500m winds. Tu et al. [39] used 330 m winds from ERA5 while quantifying emissions in the Upper Silesian Coal Basin (USCB) region in Poland, which has a mean altitude of 300 m. They found that flux estimation with 10 m and 500 m wind caused variation by -25% and 13% in flux rate, as 10 m wind was 20% lower and 500 m wind was 32% higher in comparison to the 330 m wind [39]. Hu et al. [32] used wind at 850 hPa considering Shanxi, China has many mountains and only 16% of its land surface is below 1500 m while 17% exceeds this elevation. Tu et al. [36] used 100 m wind for source rate estimations for CMM observation in China. Similarly in Australia, Sadavarte et al. [40] used boundary layer winds (~ 1000 m) for TROPOMI observations. Peng et al. [37] used a unique approach by the incorporation of the GFS and GDAS data meteorology. Therefore, for high-resolution satellite observations that primarily capture localised and high emission rates, using 10 m wind data helps reduce wind-related uncertainties. In contrast, for area-integrated mapping approaches, winds at higher altitudes provide more accurate flux estimations.

4.3. Plume Detection:

Emission estimation of any methane source first requires careful plume detection to minimise false positives and estimation errors. The methane plume detection starts with the methane column enhancement by subtracting the upwind methane mass or the background mass to the observed scene or directly calculate the methane enhancement through match filter technique. This way the methane plume images are obtained. However, there are various false positives [20], so further inspection is required and for this purpose, manual checking is mostly preferred. Varon et al. [20], while studying the coal mine methane shown the false positives over San Juan mine in New Mexico. Similarly, other studies also used the manual plume selection method to

keep any observation error as low as possible [26, 32, 40, 43, 44, 46, 62]. Another technique for plume detection is cone plume model (CPM) to access methane dispersion from localized sources. Tu et al. [39] developed this model for coal mine plumes in Poland and later Tu et al. [36] used similar approaches in Shanxi, China. Peng et al. [37] used Hybrid Single-Particle Lagrangian Integrated Trajectory (HYSPLIT) model for the plume shape and dispersion for coal mine emission estimation in China. While CPM is based on observational data, the HYSPLIT model is a dispersion model that simulates plume behaviour assuming steady-state emissions. All these methods need manual verification and has a significant number of human resources for plume modelling. In the case of a coal basin with multiple coal mines emitting daily plumes, manual detection demands significant human effort. To address this, Schuit et al. [28] developed an automated methane plume detection and monitoring system using a two-step machine learning approach. This method employs a convolutional neural network (CNN) to identify plume-like structures in methane data, followed by a support vector classifier to differentiate actual emission plumes from retrieval artifacts. Schuit et al. [28] reported detection of 581 plume over coal mine facilities using this approach.

4.4. Flux Observation and Estimation Techniques

The final and key step in studying any methane source is the application of the mass balance equation for emission rate or flux quantification. Different approaches have been employed to estimate methane emissions, each with its own strengths and limitations. These methods range from simple mass balance techniques to complex inverse modelling frameworks [19]. Comparing various source estimation processes helps in understanding the reliability of emission estimates, the impact of observational constraints, and the uncertainties associated with different methodologies. Integrated mass enhancement (IME) is the most used method for the source rate quantifications for the coal mine emission observations, and seven studies were conducted based on the IME method [20, 26, 28, 43, 44, 46, 62]. Only two studies were conducted with Cross-sectional flux (CSF) method [20, 40], and wind assign anomaly (WAS) method [36, 39], two studied used model free mass balance approach [32, 34], and one used HYSPLIT model approach [37]. For GOSAT observations, NAME Model and GOES-Chem with Bayesian outcome were utilised to get the source rate estimates [50, 51]. To further smooth out most of the observation artefacts, wind rotation plume and time averaging methods were also employed by Varon et al. [20] and Sadavarte et al. [40]. Varon et al. [20] carried out source rate quantifications using both IME and CSF methods for same mines and provided a great opportunity to compare the two methods to discuss various uncertainties and limitations for coal mine emissions. The IME and CSF methods show notable differences in their measured values across while estimating three coal mine emissions by Varion et al. [20] and IME method tends to produce higher estimates in certain cases, while the CSF method remains relatively stable considering the difference in the estimation approaches. These differences arise because the IME method is more sensitive to background concentration uncertainties and plume dispersion assumptions, while the CSF method directly integrates flux across the plume's cross-sectional area, making it less sensitive to total plume extent but potentially affected by alignment with wind direction.

Table 3: List of papers.

S.No.	Title
1	Merging TROPOMI and eddy covariance observations to quantify 5-years of daily CH4 emissions over coal-mine dominated region
2	High-resolution satellite estimates of coal mine methane emissions from local to regional scales in Shanxi, China
3	COCCON Measurements of XCO2, XCH4 and XCO over Coal Mine Aggregation Areas in Shanxi, China, and Comparison to TROPOMI and CAMS Datasets
4	Seasonal and trend variation of methane concentration over two provinces of South Africa using Sentinel-5p data
5	Unveiling Unprecedented Methane Hotspots in China's Leading Coal Production Hub: A Satellite Mapping Revelation

6	A survey of methane point source emissions from coal mines in Shanxi province of China using AHSI on board Gaofen-5B
7	Quantifying CH4emissions from coal mine aggregation areas in Shanxi, China, using TROPOMI observations and the wind-assigned anomaly method
8	Exploiting the entire near-infrared spectral range to improve the detection of methane plumes with high-resolution imaging spectrometers
9	High-resolution assessment of coal mining methane emissions by satellite in Shanxi, China
10	Automated detection and monitoring of methane super-emitters using satellite data
11	Huge CH4, NO2 and CO Emissions from Coal Mines in the Kuznetsk Basin (Russia) Detected by Sentinel-5P
12	Observed changes in China s methane emissions linked to policy drivers
13	Quantifying CH4 emissions in hard coal mines from TROPOMI and IASI observations using the wind-assigned anomaly method
14	Methane Emissions from Superemitting Coal Mines in Australia Quantified Using TROPOMI Satellite Observations
15	Mapping methane point emissions with the PRISMA spaceborne imaging spectrometer
16	Sustained methane emissions from China after 2012 despite declining coal production and rice-cultivated area
17	Investigating large methane enhancements in the U.S. San Juan Basin
18	China's coal mine methane regulations have not curbed growing emissions
19	From data to actionable insight: Monitoring fugitive methane emissions at oil and gas facilities using satellites
20	Quantifying Time-Averaged Methane Emissions from Individual Coal Mine Vents with GHGSat-D Satellite Observations
21	The added value of satellite observations of methane for understanding the contemporary methane budget

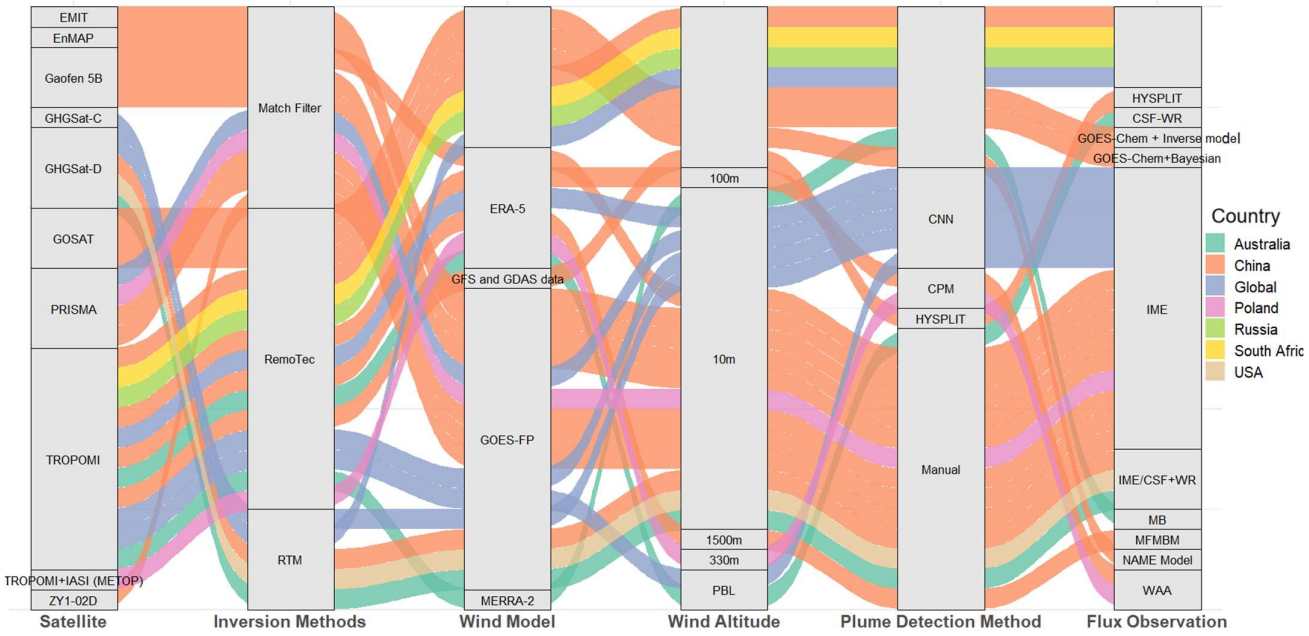

Figure 3. Alluvial plot showing relationships among satellite methane observations, analysis techniques, and basin locations. The blank column indicates absence of that step in the respective study workflow.

Quantifying methane emissions remains a challenging task, requiring precise background information. Most previous studies have relied on manual plume detection, which demands significant human effort. However, automated detection can significantly enhance quantification. Schuit et al. [28] introduced a two-step machine learning algorithm using a convolutional neural network (CNN) to autodetect methane plumes and distinguish them from artifacts. Their model, trained on TROPOMI data (pre-2021), detected 2,974 plumes, of which 20% (581) were associated with coal mines. Between 2018 and 2021, they trained the model on 828 plumes, identifying 195 plumes over mining regions. These plumes were detected across China (269), Poland (7), South Africa (50), Russia (64), Australia (46), India (55), and the USA (52). To classify the sources of methane plumes, Schuit et al. [28] utilized three high-spatial-resolution satellite instruments: GHGSat, PRISMA, and Sentinel-2. Their study estimated that coal mine emissions contribute approximately 4.7% (2.1 Tg/year) of the total global methane flux. Using the IME method, they reported a mean emission rate of 44 t/h, with individual detections ranging from 8 to 122 t/h. However, because TROPOMI has a relatively large pixel size, a single detected plume often includes emissions from multiple coal mines. In fact, high-resolution GHGSat observations showed that up to ten distinct coal mine plumes could be encompassed within a single TROPOMI detection.

5. Methane Monitoring Across Different Coal Basins and related uncertainties

Various satellite observations have been utilised for CMM monitoring and quantification across the globe. Shanxi, China, has been the most studied region due to the large number of coal mines and China's significant contribution to coal mine methane emissions [43]. Australia, Poland, the USA, Russia, and South Africa are other major regions that have been the focus of satellite-based coal mine methane emission observations. Figure 3 shows that the from satellite observation to quantification of methane has number of variable path and hence may be the reason for the variability of this final quantification and most studies have focused on a single country or basin; however, Varon et al. [20], Schuit et al. [28], and Roger et al. [62] examined coal

mine emissions across multiple countries. Here, we provide a comprehensive review of studies categorised by country, followed by a final section discussing global-scale assessments of coal mine methane emissions.

5.1. China

China's 12th Five-Year Plan set a target of utilising 8.4 billion cubic meters (5.6 Tg) of coal mine methane (CMM) by 2015 [50]. To achieve this, various policies were implemented along with incentives for CMM utilisation. However, between 2005 and 2012, CMM utilisation increased only from 0.6 to 2.3 Tg CH_4 (equivalent to 0.9–3.5 billion cubic meters) [65], falling significantly short of the 2015 goal. Miller et al. [50] conducted a total emission and trend analysis of methane from 2010 to 2015 using GOSAT data at a global scale, with a primary focus on China. The study aimed to assess the impact of policy implementation on methane emissions from coal mines in China. It also incorporated global model estimates and atmospheric inversions for source estimations. Miller et al. [50] reported an increasing methane trend in China of 1.1 ± 0.4 Tg CH_4/year, while for India, the increase was 0.7 ± 0.5 Tg CH_4/year during 2010–2015. The methane emissions trend from the coal sector assessed by Miller et al. [50] showed a rising trend between 2010 and 2015, prompting a reassessment of both satellite observation data and coal mine methane (CMM) policies. Sheng et al. [51] repeated the methane trend analysis for China using an extended observational record and an updated modelling approach with GOSAT data, aiming to verify the findings of Miller et al. [50]. They used the UK Met Office's NAME (Numerical Atmospheric Dispersion Modelling Environment), a Lagrangian particle dispersion model [69], to perform the inversions. Sheng et al. [51] reported a slow increasing trend of 0.36 ± 0.04 Tg CH_4/year during 2010–2017 and 0.5 ± 0.2 Tg CH_4/year during 2010–2015, whereas Miller et al. [50] had reported 1.1 ± 0.4 Tg CH_4/year for the same period. Sheng et al. [51] observed an increasing trend of 0.7 ± 0.3 Tg CH_4/year from 2010 to 2012 due to CMM emissions, followed by a flattening trend with a smaller growth of 0.1 ± 0.06 Tg CH_4/year from 2012 to 2017. Sheng et al. [51] also noted the coarser resolution of EDGAR v4.2, which attributed 85% of emissions to coal and mixed sources, whereas a higher-resolution national inventory by Sheng et al. [70] found that only 28% of emissions were dominated by coal and other sources.

Further, using PRISMA images, Guanter et al. [46] quantified methane emissions in the Shanxi Basin, China using advanced matched filter method. Four plumes were identified with emission rates (Q_c) of 5,900 ± 2,400 kg/h, 7,700 ± 3,100 kg/h, 8,700 ± 3,500 kg/h, and 9,600 ± 3,800 kg/h. No information is provided regarding the type of coal mine by Guanter et al. [46], however, based on the plume size and emission rate, the emissions appear to originate from the ventilation shafts of underground mines. As per the analysis by Guanter et al. [46], PRISMA observations are unable to detect emissions below 500 kg/h. Additionally, the observations showed a strong dependency on surface type, requiring special care in plume selection.

Zhang et al. [52] extended GOSAT-based methane emission estimates by assimilating high-quality surface methane measurements with previously available satellite and ground-based data for 2010–2017. The study reported an annual mean total emission rate of 54 Tg/year for China, with 50 Tg/year attributed to anthropogenic sources, closely aligning with China's official UNFCCC report (54 Tg/year for 2014). Zhang et al. [52] estimated a linear trend of 0.73 Tg/year², with an ensemble range of 0.56–0.85 Tg/year², which was higher than Sheng et al.'s [51] estimate of 0.36 ± 0.04 Tg CH_4/ year² but lower than Miller et al.'s [50] estimate of 1.1 ± 0.4 Tg CH_4/ year². The study emphasized the importance of continuous observations, as satellite-only inversion estimated an annual mean methane emission of 59 Tg CH_4/year with a positive trend of 0.16 Tg CH_4/year². The study also analysed spatial variability in coal mine methane emissions across China, finding a positive trend in Shanxi, Inner Mongolia, and northern Shanxi, which coincided with increased coal production. Conversely, a negative trend was observed in Henan and southern Shanxi, where mine closures and coal bed methane (CBM) capture and utilisation were more effective.

Peng et al. [37] estimated methane emissions in Shanxi, China, from 2019 to 2020 by assimilating TROPOMI column concentrations with plume simulations using the HYSPLIT model. Shanxi accounts for 15% of global coal production, with 239 mines producing more than 0.5 million tonnes of coal annually in 2019 [37]. A total of 112 images were processed, revealing seasonal variations, including a 14% (0.1 Tg

CH_4/month) reduction in emissions during the 2019 Spring Festival. The mean total flux observed was 8.55 ± 0.6 Tg/year (8.5 ± 0.6 Tg/year in 2019 and 8.6 ± 0.6 Tg/year in 2020). TROPOMI-based emissions were higher than PKU-CH4 v2 (5.8 ± 0.5 Tg/year) and GFEI v2 (7.3 ± 2.0 Tg/year) but closely aligned with EDGAR v6.0 (8.8 Tg/year).

Hu et al., [32] also estimated the methane emission in Shanxi, China during 2018 to 2022 using the TROPOMI observation using mass balance approaches coupled with the high-frequency eddy-covariance flux observations. They reported a 5-year mean emission of 126 ± 58.8 μg m^{-2} s^{-1} which was slightly higher than EDGAR reported (120 μg m^{-2} s^{-1}). Tu et al. [36] quantified methane emissions in Shanxi Province, China, from May 2018 to May 2023 using TROPOMI observations, wind anomaly methods, IPCC Tier 2 data, and comparisons with EDGAR v7.0 and CAMS-GLOB-ANT inventories. Contrary to previous estimates, they reported that Shanxi exceeded 1 billion tonnes of coal production in 2021, accounting for 12% of global output. The study identified 600 coal mines in Shanxi and grouped them into three regions—Yangquan, Changzhi, and Jincheng—reporting lower emissions than EDGAR v6.0.

The coal mines in the Shanxi Province of China are mostly underground mines. So, the high-resolution satellite observations were used for the detection of the coal mine plumes by He et al. [43], Han et al. [44] and Bai et al. [26]. He et al. [43] used the spectral match filter for the retrieval of the ΔXCH_4. Using the Gaofen-5 data, they are able to detect a total of 93 plumes for a total of 32 methane sources. The emissions from these point sources show a diverse range from a minimum of 761.78 ± 185.00 kg/h to a maximum of 12,729.12 ± 4658.13 kg/h and a mean emission rate of approximately 4040.30 kg/h. This study has provided information regarding various challenges associated with the satellite remote sensing in China.

Han et al. [44] conducted an extensive and detailed investigation of CMM sources across Shanxi Province, China, utilising the Advanced Hyperspectral Imager (AHSI) aboard Gaofen-5B between 2021 and 2023. They identified 138 intermittent emission events across 82 sites, collectively estimated to release 1.20 (+0.24/−0.20, 95% confidence interval) million tonnes of methane annually. The study also highlights discrepancies among EDGAR, GMM, and satellite observations, especially in northern China, due to the exclusion of CMM exploitation in recent years. It is further emphasised that high-resolution satellite observations are helpful in determining emissions from underground mines with highly concentrated emission and support the variable emission rate findings presented by He et al. [43]. Han et al. [44] also reported, for the first time, the heavy-tail characteristics of coal emissions, a feature previously observed only in oil and gas emissions. Varon et al. [20] used high-resolution satellite (GHGSat-D) observations to estimate coal mine methane emissions from the Bulianta mine in China. Applying both IME and CSF inversion approaches, they calculated emissions of 2,410 ± 1,000 kg/h and 2,450 ± 970 kg/h respectively. In contrast, the Chinese State Administration of Coal Mine Safety [71] reported only 170 kg/h during a safety assessment, a value markedly lower than the satellite-derived estimates.

Furthermore, Bai et al. [26] conducted a detailed survey of CMM in China using multiple high-resolution satellites from 2019 to 2023. The study involved observations from seven high-resolution satellites, including GHGSat and six hyperspectral missions: Gaofen-5 01 and 02, Ziyuan-1 02D, PRISMA, EnMAP, and EMIT. They later interpolated these emissions for Shanxi, China, and compared them with datasets such as PKU-CH_4 v2, GFEI, EDGAR v8.0 (2019–2022), TI 2019, INVTRO (2019–2020), and GCMT alongside observational results of the 2019–2023 mean ΔCH_4 from TROPOMI. The combined spatial interpolation of GCMT and satellite observations aligned well with the hotspots detected using TROPOMI-based ΔCH_4 observations. However, eastern Shuozhou and central Datong were underestimated by GCMT and EDGAR v8.0 (2022), while TI 2019 showed underestimation in central Shuozhou and Xinzhou. When comparing the observations presented by Bai et al. [26] for 2019–2023 with those by Han et al. [44], it is worth noting that the latter either failed to detect emissions in eastern and central Shuozhou, central Datong, and central Xinzhou, or stricter emission regulations led to a reduction in CMM. Additionally, both studies observed a decline of 20 to 30 ppb in mean ΔXCH_4 using TROPOMI between 2021 and 2023, clearly indicating the impact of the "CBM extraction first, coal mining second" policy.

5.2. Australia

Varon et al. [20] quantified coal mine methane emissions at the Appin mine, estimating a rate of 5850 ± 2360 kg/h using the IME method and 4980 ± 2100 kg/h using the CSF method, based on high-resolution satellite observations from GHGSat during the period from August 2016 to December 2018. Extrapolating the mean hourly emissions to annual emissions for the Appin coal mine resulted in an estimated annual emission of 51.19±20.67 Gg/y and 43.62±18.40 Gg/y based on IME and CSF methods. For Appin, Cardno [72] estimated emissions at ~5,200 kg/h based on coal production activity, whereas Ong et al [73] reported a higher flux of 10,800–12,600 kg/h based on ventilation flow rates. The emission rates derived from these two observational methods show a significant difference due to the difference in the basic assumption and quantification mechanism of both methods. Further, Sadavarte et al. [40] estimated coal mine emissions in the Bowen Basin, Australia, using two years of TROPOMI observations. By analysing 125 clear-sky observations over three major sources, methane emissions were quantified using the cross-sectional flux method. The estimated annual methane emissions for the three mines, which included both surface and underground operations, were 230 ± 50 Gg/y, 190 ± 60 Gg/y, and 150 ± 63 Gg/y for the period 2018–2019. Notably, the surface mine exhibited significantly higher emissions despite lower production levels (7.7 Mt in 2018-19 and 5.8 Mt in 2019-20). Palmer et al. [34] also reported the coal mine emission Bowen basin, Australia using the TROPOMI observations during 2019. Palmer et al. [34] estimated methane emissions of 3.1 ± 1.5 Mt/y and 3.3±1.5 Mt/y for Capcoal (underground and surface) and Moranbah North/Broadmeadow (underground), respectively. For Coppabella (surface) and Hail Creek (surface), the estimated emissions were 0.9 ± 0.4 Mt/y and 1.2 ± 0.6 Mt/y. Notably, the emissions reported for Hail Creek in this study were lower than those estimated by Sadavarte et al. [40], highlighting that satellite-based observations and emission quantifications can vary significantly depending on the methodology applied.

Schuit et al. [28] detected 46 coal mine-related plumes in Australia using TROPOMI satellite. They were able to identify plumes with a minimum emission rate of 4000 ± 1000 kg/h and a maximum of 72,000 ± 28,000 kg/h, with the mean emission rate being 22,826.09 ± 9,630.43 kg/h. This translates to a mean annual emission rate of 200.0 ± 84.6 Gg/y. However, satellites such as TROPOMI, with their broad spatial coverage, are not able to distinguish point sources effectively and often capture the emissions from multiple sources simultaneously. This limitation reduces its capability in coal mine emission estimation and needs more careful study.

5.3. Poland

The Upper Silesian Coal Basin (USCB) in Poland is one of the major coal-producing regions in Europe. Tu et al. [39] quantified methane emissions from the USCB between November 2017 and December 2020 using TROPOMI observations and spatial variability was examined with methane data from the Copernicus Atmosphere Monitoring Service (CAMS), including both analysis and forecast data. The plumes were analysed with a self-developed simple cone plume model to reduce the wind related uncertainties. The estimated annual methane emissions from the USCB basin were 496 ± 17 kt/yr, which closely aligned with the European Pollutant Release and Transfer Register (E-PRTR) estimate of 448 kt/yr. The study further estimated the uncertainty introduced by wind conditions, which contributed to a 13% increase in emission rates. Tu et al. [39] further leveraged IASI observations to estimate tropospheric methane concentrations while analysing emissions over the USCB region in Poland. Their study calculated a tropospheric flux of 437±27 kt CH_4 per year using combined TROPOMI and IASI datasets. However, their findings highlighted increased uncertainty in TROPOMI+IASI inversions due to complexities associated with CH_4 vertical distribution. The reported methane estimates were 40% lower than those derived from the CAMS model and the CAMS-GLOB-ANT inventory, as the latter accounts for emissions from all sectors. The results of Tu et al. [39] aligned closely with the E-PRTR inventory estimate of 448 kt/y and showed reasonable agreement with the CoMet inventory (555 kt/y). Additionally, they were comparable to prior assessments over the USCB region, which reported emission estimates varying between 9 and 79 kt/y for specific mining shafts [74] and up to 477 kt/y based on

airborne measurements [75]. Further, using CNN based approach, Schuit et al. [28] detected only seven plumes in Poland, all located in the USCB region. The observed source rates ranged from a maximum of 41,000 ± 20,000 kg/h to a minimum of 10,000 ± 4,000 kg/h. This corresponds to a mean annual emission rate of 254.04 ± 98.59 Gg/y.

5.4. Russia

Trenchev et al. [38] presented emission estimates for the Kemerovo region in Russia from May 2018 to December 2022 based on TROPOMI observations. This region contains a total of 86 coal mines spanning an area of 26,000 km². Before assessing the emission rate, the study conducted an error analysis and removed pixels that fell outside ±3σ around the median (μ), ultimately reporting a total of 339 emission events. They observed periodic occurrence of high concentration clusters of methane over the coal mine areas. The study demonstrated spatial variations in emissions; however, the authors did not carry out flux emission calculations. They also highlighted the limitations of satellite observations, noting that the high density of mines in the area prevented satellites from resolving mine-specific emissions. Schuit et al. [28] estimated methane emissions in coal mining regions of Russia, detecting plumes (64 plumes were detected related to coal) with source rates ranging from 0.2 ± 0.1 t/h to 2.4 ± 1.1 t/h using GHGSat observations, while underground coal mine vents were found to emit up to 8.8 t/h. They quantified a mean source rate of 40.4 ± 16.9 t/h using TROPOMI data. However, they also reported that a single TROPOMI-based target represents contributions from up to 10 different point sources that may cause over estimation compared to estimation from a higher resolution GHGSat observation from a coal mine area. In Russia, two outlier source rates were observed, while three plumes exhibited unusually high uncertainty based on the Schuit et al. [28] plume data.

5.5. South Africa

Sibiya et al. [35] conducted an analysis of the spatiotemporal variation of total column methane over Mpumalanga, a coal mining province, and the Eastern Cape using TROPOMI observations. The XCH_4 shows strong seasonal variation, with a declining trend from March to June and an increasing trend in the later months. During the period from 2019 to 2024, the mean concentration ranged between ~45 to 50 ppb. The study also discusses how a large coal mine in the Mpumalanga region acts as a significant source of methane emissions, which results in a higher mean XCH_4 in Mpumalanga compared to the Eastern Cape. However, the authors did not carry out any source rate analysis of coal mine-related emissions. In contrast, Schuit et al. [28] detected 50 plumes associated with coal in South Africa. The mean source rate in South Africa was 23.4 ± 9.7 t/h, based on CNN-driven plume information using TROPOMI data. The minimum and maximum emission rates observed were 7 ± 3 t/h and 59 ± 21 t/h, respectively, with a median of 21 ± 10 t/h during 2021. Only one plume was found to be outside the typical range, marking it as an outlier with an exceptionally high source rate relative to the bulk of the observations.

5.6. USA

For the United States, Varon et al. [20] used high-resolution GHGSat-D satellite observations between August 2016 and December 2018 to quantify methane emissions from the San Juan coal mine. The IME method yielded an average flux of 2,320 ± 1,050 kg/h, while the CSF method produced a slightly higher value of 2,390 ± 1,070 kg/h, about 2–3% greater than the IME estimate. The reported 1σ uncertainties (40–45%) accounted for factors such as wind speed and direction errors, model uncertainties, retrieval noise, and source variability. Comparisons with previous studies showed that aerial measurements reported lower emissions, ranging from 360 to 2,800 kg/h [76] and 1,446 kg/h [77], whereas vent flow rate estimates suggested 2,585 kg/h [78].

6. Discussions

Methane quantification involves three main steps: observation, plume detection, and quantification. These steps further categorised into six sub-components: type of satellite, satellite inversion method, wind model,

wind altitude, plume detection method, and quantification method (Figure 3). Each combination of these factors carries its own strengths, limitations, and validation requirements, ultimately influencing the accuracy of emission estimates.

Starting with satellite observations: most methane products are derived from the inversion of passive SWIR measurements, typically using the 1.6 μm absorption band of methane. However, these measurements are constrained by factors such as spectral bandwidth, signal-to-noise ratio (SNR), and atmospheric interferences (e.g., aerosols, clouds, and water vapour). Moreover, retrieval accuracy is often affected by surface reflectivity and the limited spatial resolution of current instruments, which can restrict their ability to detect small or diffuse emission sources. Satellite observations have inherent limitations in spatial and temporal coverage, as well as sensing capabilities. The blind experiments carried out by Sherwin et al. [79] highlighted the constraints of satellite observations, as identical plumes assessed by different teams showed considerable variation, with 55% of the average estimates lying within ±50% of the measured values from the control release. These challenges become even more pronounced when monitoring coal mine emissions, which are dispersed, continuous, and highly variable, making accurate quantification particularly complex.

The first-generation SWIR satellite GOSAT observes circular pixels of 10 km diameter spaced 260 km apart along the orbit track, resulting in sparse spatial coverage that requires model interpolation and introduces significant uncertainties. In recent years, higher-resolution satellite observations have become available, but various limitations persist. Using high spatial resolution observations of Gaofen-5B, methane plumes with flux rate reaching up to 0.116Tg/y were observed in Shanxi, China [43]. However, these estimates could diverge by at least two orders of magnitude from those obtained using bottom-up and indicating that such plume detections cannot be directly scaled to annual emissions [43]. TROPOMI, on the other hand, provides daily and broader spatial coverage but has a high detection limit of 10,000–25,000 kg/h, which can bias its flux estimates towards lower emission events. GaoFan-5B observation-based emissions estimates at local scale, under idealised conditions, by Bai et al. [26] performed well at small spatial scale while comparing with EDGAR data but struggle at regional scale. They also highlight the issue of data availability in both time and space and hence raised concern towards the continuous monitoring and robust trend analysis. Satellite observations capture only instantaneous plumes, whereas coal mine emissions are continuous. Consequently, extrapolating short-term plume detections to derive annual emission estimates introduces significant uncertainty and raises concerns about accuracy [26, 36].

Methane retrievals require clear-sky conditions and low aerosol loads because clouds and aerosols strongly absorb and scatter SWIR radiation, reducing measurement accuracy. So, any observation with cloud or high aerosols (Aerosols Optical Depth > 0.3) are often discarded. For example, between 2018 and 2019, TROPOMI captured only 124 clear-sky methane column observations out of roughly 500 measurements in Australia [40]. So, even a dedicated satellite with a one-day revisit rate suffers from insufficient daily coverage for annual estimates, highlighting the essential role of continuous/more frequent ground observations in reducing extrapolation uncertainties. Further challenges in satellite inversions arise due to atmospheric aerosol concentrations. For TROPOMI observations, RemoTeC, a full-physics radiative transfer model (RTM), is used to convert satellite measurements into column concentrations. In contrast, GHGSat employs a simpler RTM and relies on a proxy method for methane inversions. While RemoTeC explicitly accounts for atmospheric aerosols, proxy-based methods do not, introducing additional uncertainties in the retrieved methane concentrations.

Surface albedo is also a crucial factor affecting remote sensing of methane emissions. High albedo (>0.7) and low solar zenith angles (~0) can cause radiance levels to exceed satellite specifications, introducing biases [20]. Conversely, low-reflection surfaces (albedo <0.05), such as dark mine surfaces, pose challenges for detection. Coal mines often exhibit low albedo, reducing satellite sensitivity [20, 43]. Additionally, surface heterogeneity complicates SWIR remote sensing, as various surfaces strongly absorb in SWIR bands, requiring careful corrections, particularly in high-resolution spectroscopy. False positives in satellite methane inversion observations were reported in GaoFen-5B data due to large solar panel arrays, greenhouses, buildings, water

bodies, and moist cultivated lands [43]. Coal mines, particularly surface mines, feature highly variable albedo and topography, leading to observation artifacts due to strong SWIR absorption [20, 43].

Wind plays a critical role in the quantification of methane emissions from plume detection to final emission estimates. Accurate plume detection is often complicated by retrieval artifacts such as stripping noise, surface reflectance variations, and stray light, which can be comparable in magnitude to the methane signal itself [20]. To address these challenges, observed plumes are reoriented to a common wind direction, minimising background noise, reducing wind-related errors, and improving the accuracy of time-averaged methane enhancements [20, 43]. Plume reorientation method has been proposed to reduce such observational artifacts [20, 40]. The effectiveness of plume identification also relies on an optimal wind speed range too low, and the plume may not develop sufficiently; too high, and the plume disperses, reducing detectability [43]. Additionally, complex topography further complicates retrievals. In China, wind at 10 m, 100 m, and 1500 m scale were included which further create inconsistency while comparing these results together and with other observational studies and inventories data. The source of wind data also proved to be a critical factor, as different models were employed to generate the wind information and model winds show significant variation with respect to ground truth. For station-level winds varied significantly from 0.5 m/s to 8 m/s during GaoFen-5B overpasses, the ERA-5 model winds remained relatively stable [43]. Consequently, satellite observations indicated strong variability in the plume for the same point source and the reported difference was 10,204.71 kg/h between the minimum and maximum [43]. This suggests that averaging the plume based on limited observations may lead to significant over- or underestimation.

Finally, a major challenge in satellite-based methane observations is the inability to measure emissions at night, as all the methane observation satellites are passive sensors that rely on solar scattered or reflected radiation. The geometry, topography, and geology of a mine strongly influence emission rates, while micrometeorological conditions can cause significant variability from one source to another so the extrapolation of emissions based on instantaneous plume may lead to significant variations. Additionally, fixed satellite overpass times can introduce bias, as emissions captured at a specific time may not represent typical activity, potentially leading to overestimation or underestimation. These challenges highlight the need for a robust, continuous/more frequent methane observation methodology for coal mines and underscore the importance of integrating satellite data with ground-based measurements for reliable emission quantification.

7. Conclusions

The rise in global methane abundance and its upward trend is well acknowledged by the scientific community. However, major challenges persist in accurately quantifying methane source and sink fluxes. Coal mines remain a significant contributor to both energy production and greenhouse gas (GHG) emissions. With the growing global demand for coal, coal mine methane (CMM) emissions have also increased. Effective CMM detection and mitigation depends on precise emission accounting, and for much of the past decade, satellite observations served as the primary tool while other technologies were still under development.

Over these past 10 years, various observation and quantification approaches have been developed, with satellite remote sensing. Satellites such as TROPOMI, PRISMA, Gaofen-5, GOSAT, and GHGSat-D, are commonly used for global methane monitoring. Additionally, IASI, EMIT, EnMAP, and Ziyuan-1 02D have contributed to methane emission observations. The improvement in satellite resolution from GOSAT (10×10 km^2) to GHGSat-D (25×25 m^2) has led to reduced uncertainty in emission estimates. RemoTeC has been widely applied for TROPOMI and GOSAT inversions; however, to accelerate plume detection, direct observation-based matched-filter methods have also been developed for CMM. Flux estimation, a multi-step process involving plume detection, reorientation, and dispersion analysis, has advanced from manual detection towards automated approaches enabled by convolutional neural networks (CNNs). The minimum flux estimates are also improved from ~50 t/h of GOSAT to ~0.1 t/h for GHGSat-D. With the availability of higher-resolution satellite observations, the gap between bottom-up and top-down estimates is narrowing.

Wind conditions constitute a major source of uncertainty in emission estimates, as variations in wind speed, direction, and the altitude chosen for flux calculations can substantially influence methane

quantification. Given the complex terrain and highly heterogeneous surface conditions of mines, the choice of wind data remains a critical factor. Complex terrain and surface heterogeneity can introduce observational artifacts and false positives, necessitating the use of wind rotation methods to correct such errors. Even observations from the same satellite over the same location often yield markedly different emission estimates, largely due to variations in wind conditions. Differences in inversion methodologies further contribute to variability in emission estimates. While satellite sensors can detect concentrated plumes typically associated with underground mines, they often struggle to accurately capture the more diffuse and spatially dispersed emissions from surface operations. Moreover, because satellites generally provide only a single daily overpass that may coincide with specific mine activities rather than typical operations, extrapolating such observations can introduce substantial uncertainties, potentially leading to both over- and underestimation of total emissions on an annual basis.

China, the world's largest producer of coal [80] owing to its extensive coal mining activities, has been a central focus of methane emission studies. Satellite platforms such as GOSAT, TROPOMI, Gaofen-5, GHGSat, PRISMA, and other hyperspectral missions have been employed to monitor CMM emissions across the region. Both increasing [50] and decreasing trends [51] of CMM in China were reported initially with using low-resolution satellite observation. However, with high-resolution satellite observations, emission estimates for most undermine emission were improved however these estimates reported discrepancies with Global inventories [44]. Australia and Poland have also gained attention for their coal mine methane emissions. The limited top-down estimates have reported differences between the measured and reported emissions using TROPOMI and GHGSat-D observations. However, given the limited number of observations and the absence of ground-truth validation, such claims continue to face major uncertainties. High-resolution PRISMA satellite observations, on the other hand, were consistent with the European Pollutant Release and Transfer Register (E-PRTR) and other inventories [39]. Russia and South Africa have also been considered for CMM observations with limited estimates based on CNN approach. A few studies have also estimated CMM emissions from individual mines in the United States and India.

Nevertheless, satellite-based observations offer broad spatial coverage and unmatched capabilities to identify super-emitters. Given the existing limitations of current approaches, effective CMM mitigation requires the development of new observational strategies that integrate high-resolution satellite data with ground-based and aerial validation methods. Future efforts should focus on improving satellite retrieval algorithms, reducing wind-related uncertainties, and enhancing the synergy between multiple observational platforms. A comprehensive and multi-sensor approach will be essential for achieving more accurate methane emission assessments and implementing effective mitigation strategies.

Author Contributions:

Conceptualisation, A.C. and S.R.; methodology, A.C. and S.R.; formal analysis, A.C.; investigation, A.C. and S.R.; data curation, A.C. and S.R.; writing—original draft preparation, A.C. and S.R.; writing—review and editing, A.C. and S.R.; visualisation, A.C.; supervision, S.R.; All authors have read and agreed to the published version of the manuscript.

Funding: This research is funded by the Australian Coal Industry's Research Program (ACARP), Project Number: C37002, titled: Methane Matters: Updates on Relevant Advances for Coal Mine Emissions.

Data Availability Statement:

The data will be provided on request.

Conflicts of Interest

The authors declare no conflicts of interest.

References

1. Montzka, S.A.; Dlugokencky, E.J.; Butler, J.H. Non-CO_2 greenhouse gases and climate change. *Nature* 2011, *476*, 43–50.
2. Touma, D.; Stevenson, S.; Lehner, F.; Coats, S. Human-driven greenhouse gas and aerosol emissions cause distinct regional impacts on extreme fire weather. *Nature Communications* 2021, *12*, 212.
3. Mostefaoui, M.; Ciais, P.; McGrath, M.J.; Peylin, P.; Patra, P.K.; Ernst, Y. Greenhouse gas emissions and their trends over the last 3 decades across Africa. *Earth System Science Data* 2024, *16*, 245–275.
4. Pörtner, H.O.; Roberts, D.C.; Poloczanska, E.S.; Mintenbeck, K.; Tignor, M.; Alegría, A.; Craig, M.; Langsdorf, S.; Löschke, S.; Möller, V.; Okem, A. In *IPCC Sixth Assessment Report—Climate Change 2022: Impacts, Adaptation and Vulnerability, Contribution of Working Group II*; IPCC: Geneva, Switzerland, 2022.
5. Price, J.; Warren, R.; Forstenhäusler, N. Biodiversity losses associated with global warming of 1.5 to 4 °C above pre-industrial levels in six countries. *Climatic Change* 2024, *177*, 47.
6. United Nations Framework Convention on Climate Change (UNFCCC). *The Paris Agreement*; 2015. Available online: https://unfccc.int/process-and-meetings/the-paris-agreement/the-paris-agreement (accessed on 8 January 2025).
7. United Nations Environment Programme (UNEP). *Emissions Gap Report 2022*; UNEP: Nairobi, Kenya, 2022. Available online: http://www.unep.org/resources/emissions-gap-report-2022 (accessed on 8 January 2025).
8. European Environment Agency (EEA). *Trends and Projections in Europe 2024*; EEA: Copenhagen, Denmark, 2024. Available online: https://www.eea.europa.eu/en/analysis/publications/trends-and-projections-in-europe-2024 (accessed on 8 January 2025).
9. Wuebbles, D.J.; Hayhoe, K. Atmospheric methane and global change. *Earth-Science Reviews* 2002, *57*, 177–210.
10. International Energy Agency (IEA). *Global Methane Tracker 2022*; IEA: Paris, France, 2022. Available online: https://www.iea.org/reports/global-methane-tracker-2022 (accessed on 8 January 2025).
11. Nisbet, E.G.; Fisher, R.E.; Lowry, D.; France, J.L.; Allen, G.; Bakkaloglu, S.; Broderick, T.J.; Cain, M.; Coleman, M.; Fernandez, J.; Forster, G. Methane mitigation: Methods to reduce emissions, on the path to the Paris Agreement. *Rev. Geophys.* 2020, 58, e2019RG000675.
12. Karakurt, I.; Aydin, G.; Aydiner, K. Sources and mitigation of methane emissions by sectors: A critical review. *Renew. Energy* 2012, 39, 40–48.
13. International Energy Agency (IEA). Global Methane Tracker 2024; IEA: Paris, France, 2024. Available online: https://www.iea.org/data-and-statistics/charts/sources-of-methane-emissions-2023-2 (accessed on 14 April 2025).
14. US EPA Coalbed Methane Outreach Program (CMOP). About Coal Mine Methane. 2025. Available online: https://www.epa.gov/cmop/about-coal-mine-methane (accessed on 14 April 2025).
15. Zhao, W.; Zhao, D.; Wang, K.; Fan, L.; Zhao, Z.; Dong, H.; Shu, L. Will greenhouse gas emissions increase with mining depth in coal mines? An analysis of gas occurrence under varying in-situ stress conditions. *Sci. Total Environ.* 2024, 945, 173957.
16. National Greenhouse and Energy Reporting (NGER). Estimating Emissions and Energy from Coal Mining: Guideline; Clean Energy Regulator: Canberra, Australia, 2024. Available online: https://cer.gov.au/document/estimating-emissions-and-energy-coal-mining-guideline (accessed on 16 March 2025).
17. Zhang, S.; Ma, J.; Zhang, X.; Guo, C. Atmospheric remote sensing for anthropogenic methane emissions: Applications and research opportunities. *Sci. Total Environ.* 2023, 893, 164701.
18. Varon, D.J.; McKeever, J.; Jervis, D.; Maasakkers, J.D.; Pandey, S.; Houweling, S.; Aben, I.; Scarpelli, T.; Jacob, D.J. Satellite discovery of anomalously large methane point sources from oil/gas production. *Geophys. Res. Lett.* 2019, 46, 13507–13516.

19. Varon, D.J.; Jacob, D.J.; McKeever, J.; Jervis, D.; Durak, B.O.; Xia, Y.; Huang, Y. Quantifying methane point sources from fine-scale satellite observations of atmospheric methane plumes. *Atmos. Meas. Tech.* 2018, 11, 5673–5686.
20. Varon, D.J.; Jacob, D.J.; Jervis, D.; McKeever, J. Quantifying time-averaged methane emissions from individual coal mine vents with GHGSat-D satellite observations. *Environ. Sci. Technol.* 2020, 54, 10246–10253.
21. Roger, J.; Guanter, L.; Gorroño, J.; Irakulis-Loitxate, I. Exploiting the entire near-infrared spectral range to improve the detection of methane plumes with high-resolution imaging spectrometers. *Atmos. Meas. Tech. Discuss.* 2023, pp.1–21.
22. Alicandro, M.; Candigliota, E.; Dominici, D.; Immordino, F.; Masin, F.; Pascucci, N.; Quaresima, R.; Zollini, S. Hyperspectral PRISMA and Sentinel-2 Preliminary Assessment Comparison in Alba Fucens and Sinuessa Archaeological Sites (Italy). *Land* 2022, 11, 2070.
23. Popescu, M.; de León, J.; Goldberg, H.; Kovács, G.; Ruggiu, L.K.; Nagy, B.; Prodan, G.P.; Grieger, B.; Kohout, T.; Licandro, J.; Karatekin, Ö. Hyperspectral imaging of meteorites using the HyperScout-H instrument. *Copernicus Meetings* 2024, No. EPSC2024-586.
24. De Luca, G.; Carotenuto, F.; Genesio, L.; Pepe, M.; Toscano, P.; Boschetti, M.; Miglietta, F.; Gioli, B. Improving PRISMA hyperspectral spatial resolution and geolocation by using Sentinel-2: Development and test of an operational procedure in urban and rural areas. ISPRS J. Photogramm. *Remote Sens.* 2024, 215, 112–135.
25. Miller, C.C.; Roche, S.; Wilzewski, J.S.; Liu, X.; Chance, K.; Souri, A.H.; Conway, E.; Luo, B.; Samra, J.; Hawthorne, J.; Sun, K. Methane retrieval from MethaneAIR using the CO_2 proxy approach: A demonstration for the upcoming MethaneSAT mission. *Atmos. Meas. Tech.* 2024, 17, 5429–5454.
26. Bai, S.; Zhang, Y.; Li, F.; Yan, Y.; Chen, H.; Feng, S.; Jiang, F.; Sun, S.; Wang, Z.; Zhou, C.; Zhou, W. High-resolution satellite estimates of coal mine methane emissions from local to regional scales in Shanxi, China. *Sci. Total Environ.* 2024, 950, 175446.
27. Joyce, P.; Ruiz Villena, C.; Huang, Y.; Webb, A.; Gloor, M.; Wagner, F.H.; Chipperfield, M.P.; Barrio Guilló, R.; Wilson, C.; Boesch, H. Using a deep neural network to detect methane point sources and quantify emissions from PRISMA hyperspectral satellite images. *Atmos. Meas. Tech.* 2023, 16, 2627–2640.
28. Schuit, B.J.; Maasakkers, J.D.; Bijl, P.; Mahapatra, G.; Van den Berg, A.W.; Pandey, S.; Lorente, A.; Borsdorff, T.; Houweling, S.; Varon, D.J.; McKeever, J. Automated detection and monitoring of methane super-emitters using satellite data. *Atmos. Chem. Phys. Discuss.* 2023, pp.1–47.
29. Hu, H.; Hasekamp, O.; Butz, A.; Galli, A.; Landgraf, J.; Aan de Brugh, J.; Borsdorff, T.; Scheepmaker, R.; Aben, I. The operational methane retrieval algorithm for TROPOMI. *Atmos. Meas. Tech.* 2016, 9, 5423–5440.
30. Hu, H.; Landgraf, J.; Detmers, R.; Borsdorff, T.; Aan de Brugh, J.; Aben, I.; Butz, A.; Hasekamp, O. Toward global mapping of methane with TROPOMI: First results and intersatellite comparison to GOSAT. *Geophys. Res. Lett.* 2018, 45, 3682–3689.
31. Lorente, A.; Borsdorff, T.; Butz, A.; Hasekamp, O.; Aan de Brugh, J.; Schneider, A.; Wu, L.; Hase, F.; Kivi, R.; Wunch, D.; Pollard, D.F. Methane retrieved from TROPOMI: Improvement of the data product and validation of the first 2 years of measurements. *Atmos. Meas. Tech.* 2021, 14, 665–688.
32. Hu, W.; Qin, K.; Lu, F.; Li, D.; Cohen, J.B. Merging TROPOMI and eddy covariance observations to quantify 5-years of daily CH4 emissions over coal-mine dominated region. *Int. J. Coal Sci. Technol.* 2024, 11, 56.
33. Tu, Q.; Hase, F.; Qin, K.; Alberti, C.; Lu, F.; Bian, Z.; Cao, L.; Fang, J.; Gu, J.; Guan, L.; Jiang, Y. COCCON Measurements of XCO2, XCH4 and XCO over Coal Mine Aggregation Areas in Shanxi, China, and Comparison to TROPOMI and CAMS Datasets. *Remote Sens.* 2024, 16, 21.

34. Palmer, P.I.; Feng, L.; Lunt, M.F.; Parker, R.J.; Bösch, H.; Lan, X.; Lorente, A.; Borsdorff, T. The added value of satellite observations of methane for understanding the contemporary methane budget. *Philos. Trans. R. Soc. A* 2021, 379, 20210106.
35. Sibiya, S.S.; Mhangara, P.; Shikwambana, L. Seasonal and trend variation of methane concentration over two provinces of South Africa using Sentinel-5p data. *Environ. Monit. Assess.* 2024, 196, 713.
36. Tu, Q.; Hase, F.; Qin, K.; Cohen, J.B.; Khosrawi, F.; Zou, X.; Schneider, M.; Lu, F. Quantifying CH4 emissions from coal mine aggregation areas in Shanxi, China, using TROPOMI observations and the wind-assigned anomaly method. *Atmos. Chem. Phys.* 2024, 24, 4875–4894.
37. Peng, S.; Giron, C.; Liu, G.; D'Aspremont, A.; Benoit, A.; Lauvaux, T.; Lin, X.; de Almeida Rodrigues, H.; Saunois, M.; Ciais, P. High-resolution assessment of coal mining methane emissions by satellite in Shanxi, China. *iScience* 2023, 26, 12.
38. Trenchev, P.; Dimitrova, M.; Avetisyan, D. Huge CH4, NO2 and CO Emissions from Coal Mines in the Kuznetsk Basin (Russia) Detected by Sentinel-5P. *Remote Sens.* 2023, 15, 1590.
39. Tu, Q.; Schneider, M.; Hase, F.; Khosrawi, F.; Ertl, B.; Necki, J.; Dubravica, D.; Diekmann, C.J.; Blumenstock, T.; Fang, D. Quantifying CH4 emissions in hard coal mines from TROPOMI and IASI observations using the wind-assigned anomaly method. *Atmos. Chem. Phys.* 2022, 22, 9747–9765.
40. Sadavarte, P.; Pandey, S.; Maasakkers, J.D.; Lorente, A.; Borsdorff, T.; Denier van der Gon, H.; Houweling, S.; Aben, I. Methane emissions from superemitting coal mines in Australia quantified using TROPOMI satellite observations. *Environ. Sci. Technol.* 2021, 55, 16573–16580.
41. Liu, Y.N.; Sun, D.X.; Hu, X.N.; Ye, X.; Li, Y.D.; Liu, S.F.; Cao, K.Q.; Chai, M.Y.; Zhang, J.; Zhang, Y.; Sun, W.W. The advanced hyperspectral imager: Aboard China's GaoFen-5 satellite. *IEEE Geosci. Remote Sens. Mag.* 2019, 7, 23–32.
42. Irakulis-Loitxate, I.; Guanter, L.; Liu, Y.N.; Varon, D.J.; Maasakkers, J.D.; Zhang, Y.; Chulakadabba, A.; Wofsy, S.C.; Thorpe, A.K.; Duren, R.M.; Frankenberg, C. Satellite-based survey of extreme methane emissions in the Permian basin. *Sci. Adv.* 2021, 7, eabf4507.
43. He, Z.; Gao, L.; Liang, M.; Zeng, Z.C. A survey of methane point source emissions from coal mines in Shanxi province of China using AHSI on board Gaofen-5B. *Atmos. Meas. Tech.* 2024, 17, 2937–2956.
44. Han, G.; Pei, Z.; Shi, T.; Mao, H.; Li, S.; Mao, F.; Ma, X.; Zhang, X.; Gong, W. Unveiling unprecedented methane hotspots in China's leading coal production hub: A satellite mapping revelation. *Geophys. Res. Lett.* 2024, 51, e2024GL109065.
45. Cogliati, S.; Sarti, F.; Chiarantini, L.; Cosi, M.; Lorusso, R.; Lopinto, E.; Miglietta, F.; Genesio, L.; Guanter, L.; Damm, A.; Pérez-López, S. The PRISMA imaging spectroscopy mission: overview and first performance analysis. *Remote Sens. Environ.* 2021, 262, 112499.
46. Guanter, L.; Irakulis-Loitxate, I.; Gorroño, J.; Sánchez-García, E.; Cusworth, D.H.; Varon, D.J.; Cogliati, S.; Colombo, R. Mapping methane point emissions with the PRISMA spaceborne imaging spectrometer. *Remote Sens. Environ.* 2021, 265, 112671.
47. Gauthier, J.F.; Germain, S. From Data to Actionable Insight: Monitoring Fugitive Methane Emissions at Oil and Gas Facilities Using Satellites. In Proceedings of the Abu Dhabi International Petroleum Exhibition and Conference, Abu Dhabi, UAE, 11–14 November 2019.
48. Jervis, D.; McKeever, J.; Durak, B.O.; Sloan, J.J.; Gains, D.; Varon, D.J.; Ramier, A.; Strupler, M.; Tarrant, E. The GHGSat-D imaging spectrometer. *Atmos. Meas. Tech.* 2021, 14, 2127–2140.
49. Kuze, A.; Suto, H.; Shiomi, K.; Kawakami, S.; Tanaka, M.; Ueda, Y.; Deguchi, A.; Yoshida, J.; Yamamoto, Y.; Kataoka, F.; Taylor, T.E. Update on GOSAT TANSO-FTS performance, operations, and data products after more than 6 years in space. *Atmos. Meas. Tech.* 2016, 9, 2445–2461.
50. Miller, S.M.; Michalak, A.M.; Detmers, R.G.; Hasekamp, O.P.; Bruhwiler, L.M.; Schwietzke, S. China's coal mine methane regulations have not curbed growing emissions. *Nat. Commun.* 2019, 10, 303.

51. Sheng, J.; Tunnicliffe, R.; Ganesan, A.L.; Maasakkers, J.D.; Shen, L.; Prinn, R.G.; Song, S.; Zhang, Y.; Scarpelli, T.; Bloom, A.A.; Rigby, M. Sustained methane emissions from China after 2012 despite declining coal production and rice-cultivated area. *Environ. Res. Lett.* 2021, 16, 104018.
52. Zhang, Y.; Fang, S.; Chen, J.; Lin, Y.; Chen, Y.; Liang, R.; Jiang, K.; Parker, R.J.; Boesch, H.; Steinbacher, M.; Sheng, J.X. Observed changes in China's methane emissions linked to policy drivers. *Proc. Natl. Acad. Sci. USA* 2022, *119*, e2202742119.
53. García, O.E.; Schneider, M.; Ertl, B.; Sepúlveda, E.; Borger, C.; Diekmann, C.; Wiegele, A.; Hase, F.; Barthlott, S.; Blumenstock, T.; Raffalski, U. The MUSICA IASI CH4 and N2O products and their comparison to HIPPO, GAW and NDACC FTIR references. *Atmos. Meas. Tech.* 2018, 11, 4171–4215.
54. Diekmann, C.J.; Schneider, M.; Ertl, B.; Hase, F.; García, O.; Khosrawi, F.; Sepúlveda, E.; Knippertz, P.; Braesicke, P. The global and multi-annual MUSICA IASI {H2O, δD} pair dataset. *Earth Syst. Sci. Data* 2021, 13, 5273–5292.
55. Schneider, M.; Ertl, B.; Diekmann, C.J.; Khosrawi, F.; Weber, A.; Hase, F.; Höpfner, M.; García, O.E.; Sepúlveda, E.; Kinnison, D. Design and description of the MUSICA IASI full retrieval product. *Earth Syst. Sci. Data Discuss.* 2021, 2021, 1–51.
56. Schneider, M.; Ertl, B.; Tu, Q.; Diekmann, C.J.; Khosrawi, F.; Röhling, A.N.; Hase, F.; Dubravica, D.; García, O.E.; Sepúlveda, E.; Borsdorff, T. Synergetic use of IASI profile and TROPOMI total-column level 2 methane retrieval products. *Atmos. Meas. Tech.* 2022, 15, 4339–4371.
57. Butz, A.; Hasekamp, O.P.; Frankenberg, C.; Aben, I. Retrievals of atmospheric CO2 from simulated space-borne measurements of backscattered near-infrared sunlight: accounting for aerosol effects. *Appl. Opt.* 2009, 48, 3322–3336.
58. Hasekamp, O.P.; Butz, A. Efficient calculation of intensity and polarization spectra in vertically inhomogeneous scattering and absorbing atmospheres. *J. Geophys. Res. Atmos.* 2008, *113*, D20309.
59. Schepers, D.; Guerlet, S.; Butz, A.; Landgraf, J.; Frankenberg, C.; Hasekamp, O.; Blavier, J.F.; Deutscher, N.M.; Griffith, D.W.T.; Hase, F.; Kyro, E.; Morino, I.; Sherlock, V.; Sussmann, R.; Aben, I. Methane retrievals from Greenhouse Gases Observing Satellite (GOSAT) shortwave infrared measurements: Performance comparison of proxy and physics retrieval algorithms. *J. Geophys. Res. Atmos.* 2012, *117*, D10307.
60. Thompson, D.R.; Leifer, I.; Bovensmann, H.; Eastwood, M.; Fladeland, M.; Frankenberg, C.; Gerilowski, K.; Green, R.O.; Kratwurst, S.; Krings, T.; Luna, B. Real-time remote detection and measurement for airborne imaging spectroscopy: A case study with methane. *Atmos. Meas. Tech.* 2015, *8*, 4383–4397.
61. Thompson, R.L.; Stohl, A.; Zhou, L.X.; Dlugokencky, E.; Fukuyama, Y.; Tohjima, Y.; Kim, S.Y.; Lee, H.; Nisbet, E.G.; Fisher, R.E.; Lowry, D. Methane emissions in East Asia for 2000–2011 estimated using an atmospheric Bayesian inversion. *J. Geophys. Res. Atmos.* 2015, *120*, 4352–4369.
62. Roger, J.; Irakulis-Loitxate, I.; Gorroño, J.; Valverde, A.; Guanter, L. The Improvement of Methane Plume Detection with High-Resolution Satellite-Based Imaging Spectrometers. *Environ. Sci. Proc.* 2024, *28*, 20.
63. Hersbach, H.; Bell, B.; Berrisford, P.; Hirahara, S.; Horányi, A.; Muñoz-Sabater, J.; Nicolas, J.; Peubey, C.; Radu, R.; Schepers, D.; Simmons, A. The ERA5 global reanalysis. *Q. J. R. Meteorol. Soc.* 2020, *146*, 1999–2049.
64. Ayasse, A.K.; Thorpe, A.K.; Roberts, D.A.; Funk, C.C.; Dennison, P.E.; Frankenberg, C.; Steffke, A.; Aubrey, A.D. Evaluating the Effects of Surface Properties on Methane Retrievals Using a Synthetic Airborne Visible/Infrared Imaging Spectrometer Next Generation (AVIRIS-NG) Image. *Remote Sens. Environ.* 2018, *215*, 386–397.
65. Huang, S. Current Situations of CBM/CMM Recovery and Utilization & Methane Emission Reduction in China. *Glob. Methane Initiat. Expo* 2013, pp. 12–15.
66. Bergamaschi, P.; Houweling, S.; Segers, A.; Krol, M.; Frankenberg, C.; Scheepmaker, R.A.; Dlugokencky, E.; Wofsy, S.C.; Kort, E.A.; Sweeney, C.; et al. Atmospheric CH_4 in the First Decade of

the 21st Century: Inverse Modeling Analysis Using SCIAMACHY Satellite Retrievals and NOAA Surface Measurements. *J. Geophys. Res. Atmos.* 2013, *118*, 7350–7369.
67. Bruhwiler, L.; Dlugokencky, E.; Masarie, K.; Ishizawa, M.; Andrews, A.; Miller, J.; Sweeney, C.; Tans, P.; Worthy, D. CarbonTracker-CH_4: An Assimilation System for Estimating Emissions of Atmospheric Methane. *Atmos. Chem. Phys.* 2014, *14*, 8269–8293.
68. Yuan, J.; Xiang, J.; Liu, D.; Kang, H.; He, T.; Kim, S.; Lin, Y.; Freeman, C.; Ding, W. Rapid Growth in Greenhouse Gas Emissions from the Adoption of Industrial-Scale Aquaculture. *Nat. Clim. Chang.* 2019, *9*, 318–322.
69. Manning, A.J.; O'Doherty, S.; Jones, A.R.; Simmonds, P.G.; Derwent, R.G. Estimating UK Methane and Nitrous Oxide Emissions from 1990 to 2007 Using an Inversion Modeling Approach. *J. Geophys. Res. Atmos.* 2011, *116*, D02305.
70. Sheng, J.; Song, S.; Zhang, Y.; Prinn, R.G.; Janssens-Maenhout, G. Bottom-Up Estimates of Coal Mine Methane Emissions in China: A Gridded Inventory, Emission Factors, and Trends. *Environ. Sci. Technol. Lett.* 2019, *6*, 473–478.
71. China State Administration of Coal Mine Safety (CSACMS). *Compilation of National Coal Mine Gas Level Identification for 2011*; National Coal Mine Safety Supervision Bureau: Beijing, China, 2019.
72. Cardno. Environmental Assessment Appin Colliery Area 7 Goaf Gas Drainage Project. 2009. Available online: https://www.south32.net/docs/default-source/illawarra-coal/bulli-seam-operations/appin/appin-surface-gasmanagement-project---enviro-asse/environmental-assessment-appinsurface-gas-management-project.pdf?sfvrsn=321a9200_4 (accessed on 20 May 2025).
73. Ong, C.; Day, S.; Halliburton, B.; Marvig, P.; White, S. Regional Methane Emissions in NSW CSG Basins. Unpublished Report, 2017.
74. Krautwurst, S.; Gerilowski, K.; Borchardt, J.; Wildmann, N.; Galkowski, M.; Swolkien, J.; Marshall, J.; Fiehn, A.; Roiger, A.; Ruhtz, T.; et al. Quantification of CH_4 Coal Mining Emissions in Upper Silesia by Passive Airborne Remote Sensing Observations with the MAMAP Instrument During CoMet. *Atmos. Chem. Phys. Discuss.* 2021, 1–39.
75. Fiehn, A.; Kostinek, J.; Eckl, M.; Klausner, T.; Gałkowski, M.; Chen, J.; Gerbig, C.; Röckmann, T.; Maazallahi, H.; Schmidt, M.; Korbeń, P. Estimating CH_4, CO_2, and CO Emissions from Coal Mining and Industrial Activities in the Upper Silesian Coal Basin Using an Aircraft-Based Mass Balance Approach. *Atmos. Chem. Phys. Discuss.* 2020, 1–33.
76. Frankenberg, C.; Thorpe, A.K.; Thompson, D.R.; Hulley, G.; Kort, E.A.; Vance, N.; Borchardt, J.; Krings, T.; Gerilowski, K.; Sweeney, C.; Conley, S. Airborne Methane Remote Measurements Reveal Heavy-Tail Flux Distribution in Four Corners Region. *Proc. Natl. Acad. Sci. USA* 2016, *113*, 9734–9739.
77. Smith, M.L.; Gvakharia, A.; Kort, E.A.; Sweeney, C.; Conley, S.A.; Faloona, I.; Newberger, T.; Schnell, R.; Schwietzke, S.; Wolter, S. Airborne Quantification of Methane Emissions Over the Four Corners Region. *Environ. Sci. Technol.* 2017, *51*, 5832–5837.
78. United States Environmental Protection Agency (EPA). Facility Level Information on Greenhouse Gases Tool (FLIGHT). 2017. Available online: https://ghgdata.epa.gov/ghgp/service/html/2017?id=1009342&et=undefined (accessed on 20 May 2025).
79. Sherwin, E. D.; El Abbadi, S. H.; Burdeau, P. M.; Zhang, Z.; Chen, Z.; Rutherford, J. S.; Chen, Y.; Brandt, A. R. Single-Blind Test of Nine Methane-Sensing Satellite Systems from Three Continents. Atmos. Meas. Tech. 2024, 17 (2), 765–782. https://doi.org/10.5194/amt-17-765-2024.
80. Worldometers (2025) *Coal Production by Country*. Worldometers. Available online: https://www.worldometers.info/coal/coal-production-by-country/ (accessed on 15 September 2025).